

# Confined Catalytic Janus Swimmers in a Crowded Channel: Geometry-Driven Rectification Transients and Directional Locking

Hailing Yu, Andrii Kopach, Vyacheslav R. Misko, Anna A. Vasyleko, Denys Makarov, Fabio Marchesoni, Franco Nori, Larysa Baraban,\* and Gianaurelio Cuniberti

**S**elf-propelled Janus particles, acting as microscopic vehicles, have the potential to perform complex tasks on a microscopic scale, suitable, e.g., for environmental applications, on-chip chemical information processing, or *in vivo* drug delivery. Development of these smart nanodevices requires a better understanding of how synthetic swimmers move in crowded and confined environments that mimic actual biosystems, e.g., network of blood vessels. Here, the dynamics of self-propelled Janus particles interacting with catalytically passive silica beads in a narrow channel is studied both experimentally and through numerical simulations. Upon varying the area density of the silica beads and the width of the channel, active transport reveals a number of intriguing properties, which range from distinct bulk and boundary-free diffusivity at low densities, to directional “locking” and channel “unclogging” at higher densities, whereby a Janus swimmer is capable of transporting large clusters of passive particles.

## 1. Introduction

Artificial machines, or “microswimmers,” mimicking the motion of living objects,<sup>[1]</sup> are extensively studied both experimentally and theoretically.<sup>[2–20]</sup> The effort of both experimentalists and theoreticians has been intensifying in the anticipation of ground-breaking applications to environmental<sup>[21]</sup> and medical sciences<sup>[22]</sup> and nanotechnology

at large. Some of the promising research directions include understanding the motion of living objects like ciliated protozoa,<sup>[1]</sup> performing microsurgery, precise delivery of drugs, eliminating cancer cells,<sup>[9,19]</sup> and enhancement of the bioanalyte detection.<sup>[7]</sup> Apart from the life science inspired applications, well controllable autonomously moving objects can make a strong input into the devices and systems relying on the chemical computing and information processing, acting as

H. Yu, A. Kopach, Dr. L. Baraban, Prof. G. Cuniberti  
Institute for Materials Science and Max Bergmann Center of Biomaterials  
Dresden University of Technology  
01062 Dresden, Germany  
E-mail: larysa.baraban@nano.tu-dresden.de

Dr. V. R. Misko, Dr. A. A. Vasyleko  
Departement Fysica  
Universiteit Antwerpen  
B-2020 Antwerpen, Belgium

Dr. V. R. Misko, Prof. F. Marchesoni, Prof. F. Nori  
CEMS  
RIKEN  
Saitama 351-0198, Japan

DOI: 10.1002/smll.201602039

Dr. D. Makarov  
Helmholtz-Zentrum Dresden-Rossendorf e.V.  
01314 Dresden, Germany  
Prof. F. Marchesoni  
Center for Phononics and Thermal Energy Science  
School of Physics Science and Engineering  
Tongji University  
Shanghai 200092, China

Prof. F. Nori  
Physics Department  
University of Michigan  
Ann Arbor, MI 48109-1040, USA  
Dr. L. Baraban, Prof. G. Cuniberti  
Center of Advancing Electronics Dresden cfaed  
Dresden, Germany



a tetherless carrier of the chemical species in a channel or as a trigger of some logical operations. The large selection of micro- and nanoswimmers already available include catalytically driven microscopic rods,<sup>[4,5]</sup> microtubes,<sup>[7,11,23]</sup> biofunctionalized composites of polymers and carbon nanotubes,<sup>[24]</sup> as well as spherical Janus particles.<sup>[6,8,13–16,20]</sup> In addition to the typically used catalytic propulsion due to the reaction of decomposition of hydrogen peroxide, other stimuli, e.g., light,<sup>[16]</sup> ultrasound,<sup>[25]</sup> magnetic field,<sup>[15,26,27]</sup> and photochemical reactions are utilized to efficiently generate the motion of microobjects.

A property of self-propelled particles, important in view of the aforementioned applications, is their ability of transporting a “cargo,” e.g., organic and inorganic colloidal beads,<sup>[8,28–30]</sup> or even living cells.<sup>[9,31]</sup> Apart from classical upload-transportation process, a number of exciting effects, like autonomous pumping of inert particles by self-rectified Janus swimmers in asymmetric channels,<sup>[30,32,33]</sup> can be observed. While there is a solid background available to describe the behavior of microswimmers with and without a cargo in an extended liquid environment,<sup>[13,32,34–37]</sup> the dynamics of self-propelled motion in complex environments, e.g., under confinement<sup>[16]</sup> or in crowded space,<sup>[14]</sup> poses new fundamental questions as well as challenges for their practical realization.

Here, we address experimentally and through numerical simulations the behavior of catalytically driven Janus particles (swimmers) confined in straight microfluidic channels of different dimensions containing catalytically passive silica beads. The dynamics of Janus particles is studied as a function of the channel width and the density of the silica beads, by analyzing their spatial diffusion properties, i.e., trajectories and mean squared displacements (MSD). Remarkably, despite the symmetric geometry of the system under investigation, long-lived transient dynamical states may set in, where spatial symmetry is spontaneously broken. The lifetime of such states can be comparable or even larger than our observation times, namely the typical time a Janus swimmer takes to exit a finite-length channel. This can be explained in terms of directional locking of a swimmer particle by the passive ones, which leads to a much larger rotational diffusion time (and persistence length) of the swimmer. As a result, just a few or even a single Janus particle can efficiently clear up a channel of passive particles immediately suggesting a number of potential applications, e.g., for environmental wastewater cleaning or biomolecules detection with enhanced sensitivity and specificity. On the other hand, this ability to push large aggregates through narrow constrictions can bring an added value to the understanding of drug delivery processes through tissue barriers, in the human body,<sup>[38–41]</sup> or cancer cell diffusion through the vascular system, leading to metastasis formation.<sup>[39]</sup>

## 2. Results and Discussions

### 2.1. Experimental Setup

We fabricated a device with parallel straight narrow channels of different widths using a soft lithography technique based on the polydimethylsiloxane (PDMS) replica molding process

(see details in the Supporting Information). The designed microfluidic chip consists of two reservoirs connected via straight narrow channels (**Figure 1A**, top inset), formed by binding the structured PDMS together with the unstructured top PDMS layer. The width of the channels varies from 10 to 300  $\mu\text{m}$ , while the height is fixed to 20  $\mu\text{m}$ . Typically, a 100  $\mu\text{L}$  suspension of colloidal silica particles is injected into the channel structure using glass syringes connected via Teflon tubing (Figure 1B, inset).

Extended arrays of silica particles (diameter: 3  $\mu\text{m}$ , Poly Science) are fabricated following the technique by Micheletto et al.,<sup>[42]</sup> which allows to achieve well-ordered 2D colloidal crystals upon drying of the suspension solution at ambient conditions.<sup>[42,43]</sup> The catalytic properties of the particles are assured by deposition of a 25 nm thin platinum film onto the array of silica particles (Figure 1A, bottom inset). The metallic caps in the original grayscale scanning electron microscopy (SEM) image are colored in pink to have

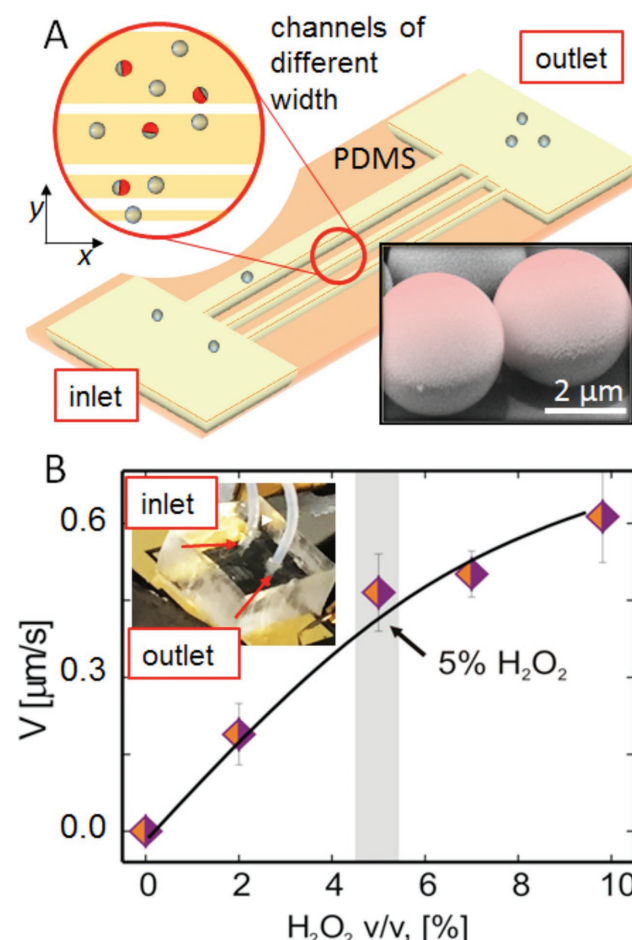


**Figure 1.** A) Schematic illustration of the entire setup enabling to monitor the dynamics of Janus particles on microfluidic chip. (Top inset) Sketch of the microfluidic channels of different widths prepared within PDMS with dispersed both Janus swimmers and plain silica particles. (Bottom inset) SEM micrograph displays the silica particles, covered by thin films of Pt, to assure the catalytic properties of the beads. B) Dependence of the velocity of a single Janus particle on the concentration of hydrogen peroxide in the solution. (Inset) Fabricated microfluidic chip installed into video-microscopy setup.

it consistent with the schematic representation of the Janus particles in the following graphs. The deposition is carried out at room temperature using magnetron sputtering in a high vacuum chamber (base pressure:  $10^{-7}$  mbar; argon (Ar) sputter pressure:  $10^{-3}$  mbar). Fabricated Janus particles are detached from the substrate by sonication and suspended in an aqueous solution of hydrogen peroxide. In the presence of hydrogen peroxide ( $\text{H}_2\text{O}_2$ ), the particles are set into motion, driven by self-diffusiophoresis, with speed determined by the concentration of  $\text{H}_2\text{O}_2$  (v/v, serial dilution) in the solution.<sup>[13,28]</sup> Note that the bubble propulsion mechanism is not dominant in the system of spherical Janus particles, since the geometry of the objects does not provide the necessary conditions for the facile nucleation of the bubbles, such as presence of the cavities or nonhomogeneous surface of the catalyst.<sup>[20]</sup> The Janus particle is propelled in the direction, opposite to the Pt cap. Catalytic Janus particles can be easily distinguished from plain silica beads by optical contrast, i.e., the difference in transmission/absorption due to the presence of the metal-covered part of silica beads. In the following, we present the quantitative analysis of their motility, caused by the decomposition of  $\text{H}_2\text{O}_2$  on the Pt caps.<sup>[44]</sup>

During the experiment, Janus particles tend to settle onto the plasma treated PDMS substrate due to gravity and then diffuse on an effectively 2D surface of the substrate. This is realized via selection of the silica as a material for the particles (amorphous silicon dioxide, density of about  $2.12 \text{ g cm}^{-3}$ ) with its density almost  $2\times$  exceeding the water density. This assures their efficient sedimentation and preferable motion at the bottom wall. The distance between the particle and the substrate, determined by the Debye screening length in deionized water, is about 100 nm.<sup>[45]</sup> Accordingly, we recorded the motion of the particles in the  $xOy$  plane, the channel being directed along the  $x$ -axis (Figure 1A).

For future reference, we characterized the dynamics of the free catalytic Janus particles far from the confining walls. The propulsion velocity  $V_f$  of a single Janus particle as a function of the concentration of  $\text{H}_2\text{O}_2$  is presented in Figure 1B. The reported values of  $V_f$  have been averaged over the speed of at least ten distinct Janus particles. In agreement with previous reports,<sup>[13,20,28]</sup> the velocity rises with the increase of the  $\text{H}_2\text{O}_2$  concentration, revealing a clear trend to saturate at high concentrations. In the following, we fix the concentration of  $\text{H}_2\text{O}_2$  at 5% in order to avoid the formation and accumulation of air bubbles inside the microfluidic chip. At the chosen  $\text{H}_2\text{O}_2$  concentration, the velocity of the Janus particles is  $V_f = 0.41 \pm 0.1 \text{ } \mu\text{m s}^{-1}$ .

## 2.2. Janus Particles in Empty Channel

After the Janus particles are placed into the microfluidic channels, they reveal two distinct regimes of motion, depending on their location with respect to the channel wall: (i) diffusion in the center of the channel and (ii) sliding along the walls, as summarized in Figure 2 (see also Video S1 in the Supporting Information).

According to the Stokes-Einstein equation,<sup>[13]</sup> the free diffusion coefficient,  $D$ , for particles with a diameter of

$3 \text{ } \mu\text{m}$ , placed in an aqueous environment with viscosity  $\eta = 8.9 \times 10^{-4} \text{ Pa s}$  at room temperature is predicted to be  $D = 0.16 \text{ } \mu\text{m}^2 \text{ s}^{-1}$ . Furthermore, the corresponding rotational diffusion time is estimated to be  $\tau_R = 19 \text{ s}$ . In the presence of a constant  $\text{H}_2\text{O}_2$  concentration, the ongoing decomposition reaction catalyzed by the Janus particle, boosts its diffusivity, hence the enhanced diffusion coefficient,  $D^*$ , and the reduced diffusion time,  $\tau_{R^*}$ , respectively.<sup>[13]</sup>

Trajectories of both a Janus and a passive particle of the same size are displayed in Figure 2A for comparison. While the passive bead experiences thermal fluctuations, the Janus particle moves ballistically at short times (see arrows), but executes Brownian motion with diffusion coefficient  $D^* = 0.23 \text{ } \mu\text{m}^2 \text{ s}^{-1}$  ( $D^* > D$ ) and characteristic  $\tau_{R^*} = 16 \text{ s}$  ( $\tau_{R^*} < \tau_R$ ) at longer times (see the fit of the MSD below in Figure 2E). The typical trajectory of a Janus swimmer moving far from the walls in a channel of width larger than  $150 \text{ } \mu\text{m}$  resembles that in the bulk. However, we observe that upon colliding with a channel wall, the swimmer slides along it and keeps doing so without inverting direction for a rather long time. Similar behavior of the active particles under confinement has been predicted by Wensink and Loewen<sup>[17]</sup> and recently shown experimentally near single straight<sup>[32]</sup> and circularly shaped wall.<sup>[33]</sup>

For channel widths smaller than  $100 \text{ } \mu\text{m}$ , the behavior of the Janus particles grows complex, as the interplay between the two motility regimes in the center and at the channel wall becomes more pronounced (see Video S1 in the Supporting Information). Further shrinking the channel below the width of  $30 \text{ } \mu\text{m}$ , leads to the apparent prevalence of the wall sliding regime (Figure 2B,C for channels, respectively, 15 and  $10 \text{ } \mu\text{m}$  wide). The rectified trajectories shown in Figure 2B,C are characterized by persistence times much longer than the estimated swimmers' rotational diffusion time in the bulk,  $\tau_R^*$ . Consequently, the directed motion of the channeled Janus swimmers reported here is attributable to a geometric suppression of their rotational diffusion. In conclusion, rectification of Janus swimmers in a microfluidic channel can be maintained for increasingly long time intervals by lowering the channel width, even without the need of, e.g., external fields to guide them.<sup>[8,45,46]</sup>

Next, we sampled more trajectories and quantitatively analyzed the velocities and MSDs of catalytically driven Janus particles in a narrow channel. Interestingly, the self-propulsion velocity,  $V$ , is found to depend on the particle location in the channel. This claim is supported by the analysis of the instantaneous and mean velocities of the swimmers sliding along the walls or moving in the center of the channel. Both regimes of motion are clearly visible in Figure 2D, where the instantaneous velocity of a particle in a  $15 \text{ } \mu\text{m}$  wide channel is plotted versus time (the corresponding trajectory is portrayed in Figure 2B).

In this experiment, a single catalytic Janus particle suspended in 5% (v/v) of  $\text{H}_2\text{O}_2$  moves with speed  $V_c = 0.34 \text{ } \mu\text{m s}^{-1}$ , which is close to the value measured for a free Janus particle,  $V_f$  ( $0.41 \text{ } \mu\text{m}$ ). Upon hitting a wall, it then switches to the sliding regime by lowering its speed to  $V_w = 0.11 \text{ } \mu\text{m s}^{-1}$ . This change of motility regime is reflected in the time dependence of the corresponding MSD curve,  $\langle \Delta r^2 \rangle$ , plotted in Figure 2E. Initially, when the Janus swimmer

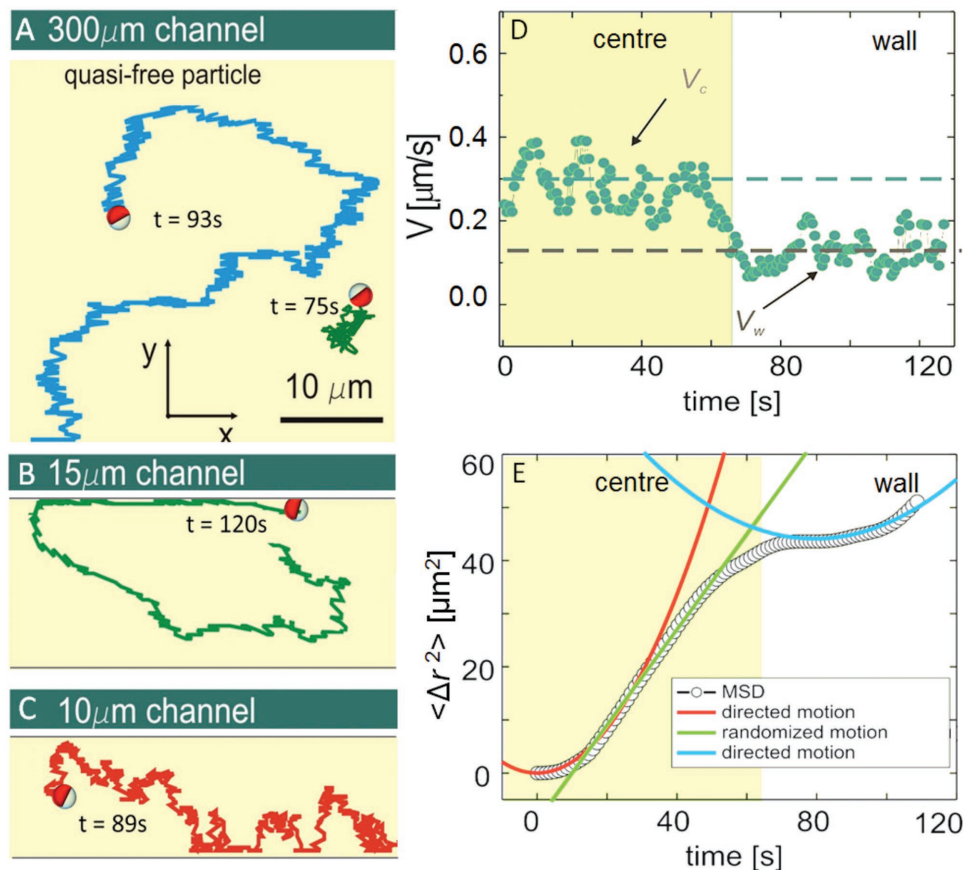


**Figure 2.** Analysis of the dynamics of the Janus swimmers in narrow channels. A) Trajectories of the Janus particle in the 300  $\mu\text{m}$  channel, resembling the free particle case; B,C) correspond to the channel width of about 15 and 10  $\mu\text{m}$ , respectively. D) Instantaneous velocities of the Janus particle in the center and at the wall are summarized. E) MSD of the Janus particle in the 15  $\mu\text{m}$  wide channel clearly determines the regimes of the motion in the center of the channel (until  $t = 50$  s) and the sliding along wall. Each part of the curve is fitted with i) parabolic and linear functions for the motion in the center (corresponding fitting functions: parabolic  $f_c(x) \sim 0.048x^2 + 0.6x$ , and linear  $f_l(x) \sim 1.33x$ ) and ii) parabolic function for the rectified motion at the wall ( $f_w(x) \sim 0.01x^2$ ). Analysis of the fit curves were used to analyze  $D^*$  and  $\tau_R^*$  from the inflection point of the curve.

is located close to the center of the channel, the MSD grows quadratically with time ( $t < 20$  s), as expected for ballistic fluctuations at  $t \ll \tau_R^*$ . For intermediate times ( $20 \text{ s} < t < 60 \text{ s}$ ), the MSD crosses over to a linear function of time. This is the signature of a normal diffusive process, which results from the angular randomization of the particle motion for  $t \gg \tau_R^*$ . Collisions with a channel wall ( $t \approx 60$  s) reorient the bead so that the main symmetry axis of the cap turns parallel to the channel (in either direction). After this adjustment, the swimmer starts sliding along the wall ( $t > 80$  s). This last dynamical change is signaled by the MSD curve reverting to quadratic time dependence, though with smaller coefficient than for short times (see Figure 2E).

Next, **Figure 3A** shows the influence of the channel's width,  $d$ , on the mean speed of Janus particles moving at the center of the channel,  $V_c$ , or sliding along the wall,  $V_w$ . These results were obtained by separately analyzing the "center" and "wall" segments of at least three recorded trajectories for each channel width (duration of about 90 s each). The results displayed here suggest that the walls of a moderately narrow channel,  $d > 30 \mu\text{m}$ , not only rectify the trajectory of a Janus particle, but also reduce its speed (from 0.34 down to  $0.12 \mu\text{m s}^{-1}$  in our microfluidic device). Indeed,  $V_w$  and  $V_c$  are

decreasing and increasing functions of  $d$ , respectively. On further decreasing the channel width,  $V_w$  and  $V_c$  approach one another. The interplay of the motion in the center and at the walls of the channel is illustrated by the curve in Figure 3B, where we plotted the particle's average speed,  $V$ , along with the full trajectory. The curve increases monotonically over the entire width domain accessible to the experiment. We attribute the observed change of the velocity and the rectification of the channeled Janus swimmer to the following reasons: (i) the transition from a 2D (near the center) to a quasi-1D motion (along the walls), (ii) higher probability of the particle to hit the wall in the case of narrower channels, and (iii) the interactions between a Janus particle and a wall. The latter can be caused by a number of factors, including the electrostatic attraction by the wall due to inhomogeneous distributions of the negative charges on the particle and wall surfaces, hydrodynamic effects, etc.

### 2.3. Simulations

The motion of a swimmer in a 2D channel is simulated by numerically integrating the Langevin equations<sup>[30,45]</sup>

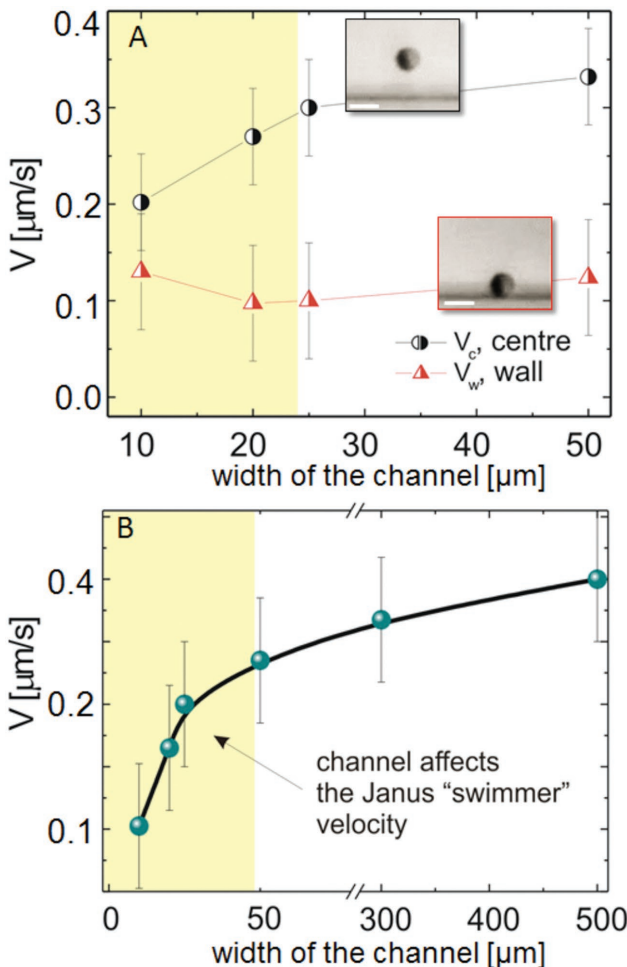


**Figure 3.** Analysis of the velocity  $V$  of the Janus swimmers in the microfluidic channel structure as a function of the channel width. A) The separated analysis of the “swimmer” velocities, moving in the center of the channel (black data points) and sliding at the wall (red data points). Insets depict the micrographs, showing the Janus swimmer particles far away and near the wall (scale bar is 4 μm). B) The mean velocity of the swimmer (averaged over the whole observation time) in channels with different widths.

$$\begin{aligned}\dot{x} &= v_0 \cos \theta + \xi_{0,x}(t) \\ \dot{y} &= v_0 \sin \theta + \xi_{0,y}(t) \\ \dot{\theta} &= \xi_{\theta}(t)\end{aligned}\quad (1)$$

where  $\xi_0(t) = (\xi_{0,x}(t), \xi_{0,y}(t))$  is a 2D thermal Gaussian noise with correlation functions  $\langle \xi_{0,i}(t) \rangle = 0$ ,  $\langle \xi_{0,i}(t) \xi_{0,j}(t) \rangle = 2D_0 \delta_{ij} \delta(t)$ , with  $i, j = x, y$ , and  $D_0$  is the translational diffusion constant of a passive particle of the same geometry at a fixed temperature. Moreover,  $\xi_\theta(t)$  is an independent 1D Gaussian noise with  $\langle \xi_\theta(t) \rangle = 0$  and  $\langle \xi_\theta(t) \xi_\theta(0) \rangle = 2D_\theta \delta(t)$ , which models the fluctuations of the propulsion angle  $\theta$  (measured here with respect to the channel axis). To model the interaction of the particles with the walls of the channel, we impose “sliding” boundary conditions, whereby a particle keeps sliding along the container boundaries, until it changes direction due to the fluctuating torque  $\xi_\theta(t)$ .<sup>[30]</sup>

We simulate the behavior of a system of  $N$  particles including  $N_m$  active swimmers and  $N_p$  passive beads. Both species are modeled by soft disks of radius  $r_0$  interacting via an elastic repulsive force.<sup>[30,45]</sup> The experimentally observed adhesion among silica beads<sup>[28,44]</sup> is modeled by an additive short-range attractive force term. The resulting interaction force of the particle pair  $i, j$  reads

$$F_{ij} = \begin{cases} k(2r_0 - |\vec{r}_i - \vec{r}_j|), & \text{if } |\vec{r}_i - \vec{r}_j| < 2r_0 \\ \kappa |\vec{r}_i - \vec{r}_j|, & \text{if } 2r_0 < |\vec{r}_i - \vec{r}_j| < 2r_0 + d_{\text{att}} \\ 0, & \text{otherwise} \end{cases} \quad (2)$$

where  $k$  and  $\kappa$  are the spring constants, respectively, of the repulsive and attractive interaction, with  $\kappa = 0.01k$ , and the range of the attractive force is  $d_{\text{att}} = 0.1r_0$ . Remarkably, we observe in **Figure 4A** that the linear slope of the MSD in intermediate time ranges ( $20 \text{ s} < t < 60 \text{ s}$ ) decreases with decreasing the channel width (see Figure S1 in the Supporting Information for qualitative comparison with the experimental results). For instance, the curve for the narrowest channel (6 μm, yellow symbols) is considerably

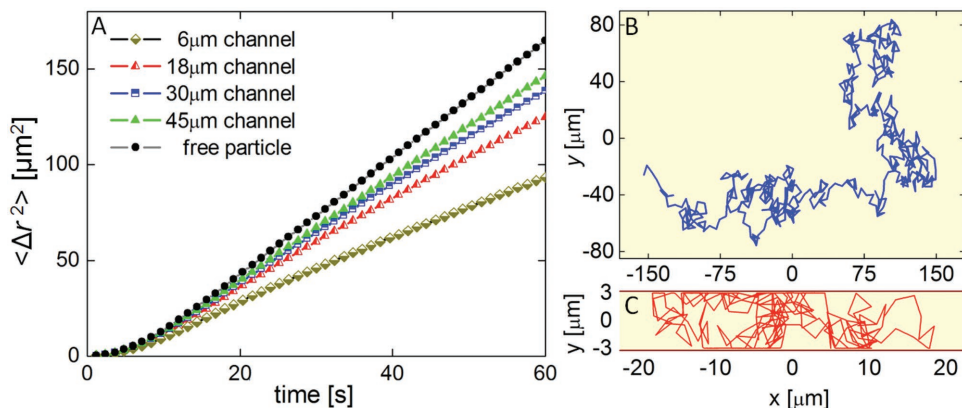


**Figure 4.** A) Simulated MSD curves of Janus swimmers confined in channels of various widths and of a free particle. B,C) Simulated trajectories of a self-propelled Janus swimmer in 2D are shown: free particle, comparable with the experimentally measured trajectory shown in (B) and in a 6 μm channel (C).

lower than those for the wider ones. This effect is the signature of the transition from a fully 2D to a quasi-1D diffusion mechanism in the channel. These results correlate with the dependence of the averaged velocity  $V$ , presented in Figure 3 as a function of the channel width  $d$ . Generally, such a transition is anticipated in time by narrowing the channel, whereas for asymptotically long times, all MSD curves attain the same slope regardless of the channel width. Examples of simulated trajectories of self-propelled particles are shown in Figure 4B for a particle in the bulk and in a 6  $\mu\text{m}$  channel (Figure 4C). In the latter case, the swimmer undergoes multiple collisions with the walls, which results in a Knudsen's diffusion process along the channel. Note that the persistence length of the self-propelled Janus particle considerably increases while sliding along the channel walls, consistently with the experimental observations (see Figure 2C).

#### 2.4. Janus Particles in Crowded Channel

To investigate the dynamics of Janus swimmers simultaneously in a crowded environment and under geometric confinement, a suspension containing a mixture of catalytic Janus beads and different concentrations of plain silica particles

with a diameter of about 3  $\mu\text{m}$  was injected into the 25  $\mu\text{m}$  wide channel. In the following, the trajectories and instantaneous velocities of the swimmers and plain beads have been analyzed as a function of the density of the passive particles in the channel (see packing fraction in the Supporting Information). Note that, in view of the low number of catalytic Janus colloids in the channel, we neglect any effect due to their density fluctuations on the packing fractions.

Depending on the density of the passive particles, we distinguish three main dynamical regimes of the active swimmers: (i) A low density regime, when the Janus beads move through the passive particles experiencing rare collisions, i.e., freely percolate between the two sides of a channel of finite length; (ii) An intermediate density regime, when a Janus particle can move through the array of passive particles or bind a passive particle cargo and drag it along, thus acting as a carrier (see Movies S2 and S3 in the Supporting Information); (iii) Finally, a high density regime, when the passive particles clog the channel and the swimmers get locked inside (Movie S4, Supporting Information). Micrographs illustrating the transition from the low to the high density regime are shown in **Figure 5A–C**.

We analyze now in detail the active colloidal transport in the first two regimes.

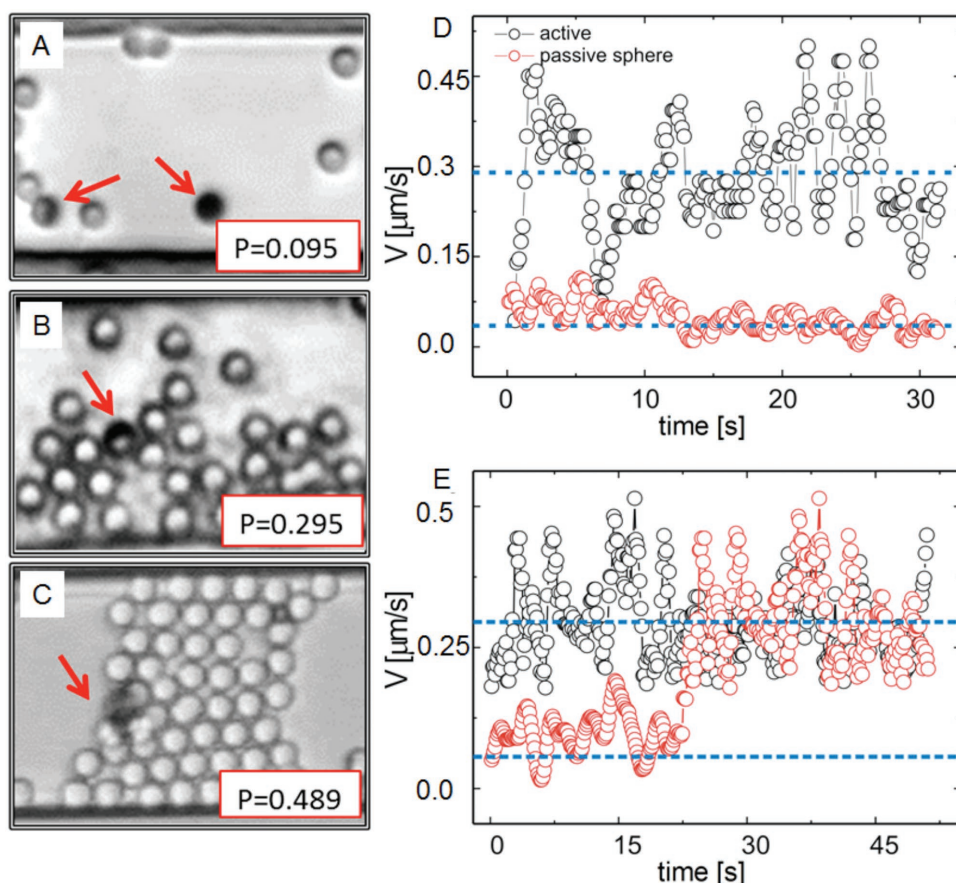


**Figure 5.** Dynamics of Janus swimmers in a crowded environment and under geometric confinement at the same time. A–C) Microscopy images of the microfluidic channels filled with both, Janus particles and passive beads for the cases of different packing densities of particles, low (a), intermediate (b), and finally high (c). D,E) Instantaneous velocities of Janus swimmers (black circles), and passive colloidal particles (red circles) for the low density particles in the channel (d) and high density (e), respectively.

#### 2.4.1. Low Density Regime

In the low density case (packing fraction of about 0.2), the behavior of the Janus swimmers is hardly modified by the presence of the passive species in the channel (Figure 5A). In particular, the long-range repulsion due to the presence of silanol groups on the surface of particles prevents the formation of the stable swimmer–cargo composites. Indeed, colloidal pairs do not approach each other close enough to perceive the stronger short-range attraction exerted by the van der Waals forces and capable of binding them.

Nevertheless, we observed the appearance of transient pairs involving both types of particles, which randomly form and dissolve, without ever accruing into stable aggregates (Figure 5A, see both cases, shown by the arrows). This is reflected in the corresponding analysis of the instantaneous velocities of both types of particles (Figure 5D). To this regard, we emphasize that the fabrication process of our Janus particles and the contamination present in the liquid may lead to a partial degradation of the negative charges on the surface of the colloids<sup>[28]</sup> and thus be responsible for the occasional formation of the carrier–cargo composites,<sup>[28,44]</sup> shown in Figure 5A.

#### 2.4.2. Intermediate and High Density Regimes

In contrast to the previous situation, a higher density of the passive species in the channel, namely, with packing fraction larger than 0.3, increases the probability of formation of carrier–cargo complexes. In this case, a Janus particle is able to propel through the matrix of plain silica beads (Figure 5B) or to form clusters bridging the channel's walls and transport them through the channel (Figure 5C and Videos S2 and S3 (Supporting Information)). In the former case (Figure 5B), a Janus particle can propel itself through the mixture of passive beads across the channel (along the  $y$ -axis). Such a transverse motion is favored by the empty room left behind by the colloidal particles as they diffuse in the longitudinal direction (along the  $x$ -axis). The latter case which involves the formation and the transport of clusters of passive beads (Figure 5C) is the most unusual. The mechanism is initiated by some active Janus swimmer that happens to rake up a bunch of surrounding passive particles upon moving along the channel ( $x$ -axis). Under the push of the swimmer and the action of the short-range pair attraction, these colloidal particles collapse into a seemingly stable cluster. As a consequence, a key role in the cluster formation is played by the combination of geometric confinement and particle–particle and particle–wall interactions (both interactions being generally of the same nature). The motion of an active Janus motor in this crowded environment is thus rather complex (see Figure 5C,E and Video S4 (Supporting Information)). The free space across the channel is very limited, and the swimmer spends most of the time either near the wall or embedded into the cluster of passive colloids. When a self-propelling swimmer collides with the particles, it becomes embedded into the colloidal ensemble by forming a number of “bonds” with the surrounding nearest silica beads. This constraint of the rotational degree of freedom considerably

increases the effective rotational diffusion time, or engagement time,  $\tau_{\text{en}} \gg \tau_R^*$ . As a rule of thumb, we expect  $\tau_{\text{en}}$  to be proportional to the number of bonds between the Janus motor and passive particles. Thus, a collision with a clogging cluster implies a nonvanishing component of the swimmer's velocity orthogonal to the surface of the cluster and, as a consequence, along the axis of the channel. The engagement mechanism locks the direction of motion for a time of the order of  $\tau_{\text{en}}$ , thus resulting in a much larger effective persistence length than for a free swimmer. In the regime of low Reynolds numbers, the dynamics of the locked system formed by the swimmer and the cluster is overdamped, which means that it drifts regardless of its total mass. Accordingly, the carrier–cargo system advances steadily as a whole, with velocity given by the longitudinal component of the propulsion speed of the locked carrier, possibly reduced by frictional forces against the channel walls. In conclusion, a carrier can transport a payload without direction inversions an effective distance much larger than its persistence length in the channel. The velocity plots of Figure 5E corroborate the proposed mechanism of carrier–cargo engagement and drift.

#### 2.4.3. Bioinspired System: Unclogging the Narrow Channel

The striking ability of confined Janus swimmers to carry along large clusters of passive particles for surprisingly long time intervals due to the locking mechanism, can prove useful for diverse environmental or biomedical applications, e.g., to unclog microchannels filled by diverse biochemical species or to model the transport processes within the vascular system. Note that human blood capillaries have dimensions of about 10–15  $\mu\text{m}$ , similar to the channels in our experiments.

To demonstrate the effect of channel unclogging, we numerically modeled the experimental situation reported above, when an active Janus motor is embedded in a cluster of passive particles and moves together with the cargo. In **Figure 6A** (top panel), a single swimmer shown by red circle pushes a cluster of sixteen passive particles (shown by black circles) from the left to the right, while three passive particles do not move. The corresponding velocities of the moving cluster (black dots) and the passive particles (red dots) are shown in stage I of Figure 6B. Two vertical dashed segments separate three distinct temporal regimes. As the colloidal aggregate approaches the isolated passive particles ( $t \approx 66$  s), it incorporates them one by one (middle and bottom panels of Figure 6A). Correspondingly, during the collisional transient, stage II of Figure 6B, the velocity of the passive particles rapidly increases, showing oscillations or even prominent dip at  $t \approx 108$  s. This behavior is due to the rearrangement of the particles before these eventually settle into the new cluster. After having rearranged themselves into a close-packed quasicrystalline structure for  $t > 108$  s, all the particles move together (Figure 6A, bottom panel) with the same velocity (Figure 6B, stage III) of the initial cluster. The collective motion of the Janus motor and the passive particles reproduces closely the active colloidal transport observed experimentally. In view of the mechanism illustrated above, we conclude that a small fraction of active motors (or even a single active motor) suffices to unclog a narrow, finite length

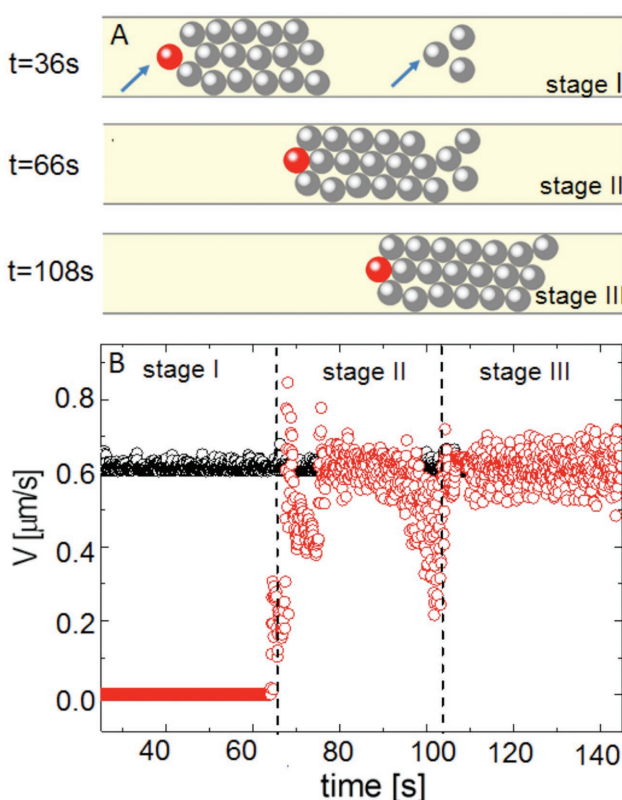


**Figure 6.** Unclogging channel filled with passive particles by an active Janus swimmer. A) Particle distribution snapshots before the collision of the moving aggregate of the Janus swimmer (red circle) and 16 passive particles (grey circles) with three unmoving particles ( $t = 36$  s), at the moment of the collision ( $t = 66$  s), and when moving as a whole cluster ( $t = 108$  s). B) The corresponding velocities of the moving aggregate driven by the Janus swimmer (black diamonds) and passive particles (red open circles).

constriction in an otherwise inaccessible region. Moreover, since such motors are autonomous, i.e., are not guided by externally applied fields, active transport of microscopic objects through narrow channels can be implemented in a fairly noninvasive manner.

### 3. Conclusion

We addressed both experimentally and numerically the behavior of confined self-propelled catalytically driven Janus particles placed in straight microfluidic channels together with passive microscopic objects. Detailed investigation of the configurations, involving the artificial Janus swimmers acting in crowded and confined environments reveal intriguing aspects of their behavior affected by the surrounding matrix, i.e., directed motion of the swimmers and the rectifying role of the narrow channels (of widths below ten particle diameters). Furthermore, the presence of the channel walls substantially influences the speed of Janus particles, leading to a decrease of the velocity at the channel walls (almost by a factor of three).

Upon combining the geometrical confinement of the swimmers with the passive microparticles filling the narrow

channels, new effects emerge. Namely, Janus beads participate in the formation and transport of large clusters of passive particles, being “built-in” into this colloidal suspension. This striking ability of Janus swimmers to transport large colloidal clusters, together with the observed mechanism of persistent directed motion, lends itself to diverse environmental or biomedical applications, i.e., to unclog or clear channels of unwanted biochemical species.

It is expected that artificial self-propelled particles will find applications to diverse emerging areas of nanotechnology, from micro- and nanorobotics, e.g., for microsurgery purposes, high sensitivity biodetection, and drug delivery, to environmental water cleaning and bio (chemo)electronics. In particular, the demonstrated experimental setup involving essentially both active and passive species, provide key ingredients for the design of novel type nanodevices. Such devices could, for instance, realize the passive transportation and detection of reagents, triggering of the reaction steps, relevant for the chemical computing, e.g., in design of chemical central processing units.<sup>[47]</sup> Taking into account the internal complexity of the natural systems, investigation of the specific aspects of the dynamics of self-driven micromachines placed into the bioinspired artificially designed spatial configurations, e.g., crowded and confined environments, is of high interest.

### Supporting Information

Supporting Information is available from the Wiley Online Library or from the author.

### Acknowledgements

H.Y., A.K., and L.B. contributed equally to this work. This work was funded in part by the European Union (ERDF) and the Free State of Saxony via the ESF project InnoMedTec, the DFG cluster for Excellence, the Center for Advancing Electronics Dresden (CFAED), and via the European Research Council under the European Union’s Seventh Framework program (FP7/2007–2013)/ERC grant agreement no. 306277. V.R.M. and A.A.V. acknowledge support from the Odysseus Program of the Flemish Government and the FWO-VI. F.N. is partially supported by the RIKEN iTHESS Project, the MURI Center for Dynamic Magneto-Optics via the AFOSR Grant No. FA9550-14-1-0040, the IMPACT program of the JST, and a Grant-in-Aid for the Scientific Research (A).

- [1] N. Silvestry-Rodriguez, K. R. Bright, D. C. Slack, D. R. Uhlmann, C. P. Gerba, *Appl. Environ. Microbiol.* **2008**, *74*, 1639.
- [2] G. A. Ozin, I. Manners, S. Fournier-Bidoz, A. Arsenault, *Adv. Mater.* **2005**, *17*, 3011.
- [3] R. Dreyfus, J. Baudry, M. L. Roper, M. Fermigier, H. A. Stone, J. Bibette, *Nature* **2005**, *437*, 862.
- [4] W. F. Paxton, S. Sundararajan, T. E. Mallouk, A. Sen, *Angew. Chem., Int. Ed.* **2006**, *45*, 5420.

- [5] W. F. Paxton, K. C. Kistler, C. C. Olmeda, A. Sen, S. K. St. Angelo, Y. Cao, T. E. Mallouk, P. E. Lammert, V. H. Crespi, *JACS* **2014**, *126*, 13424.
- [6] M. M. Stanton, C. Trichet-Paredes, S. Sánchez, *Lab Chip* **2015**, *15*, 1634.
- [7] S. Balasubramanian, D. Kagan, C.-M. Jack Hu, S. Campuzano, M. J. Lobo-Castanon, N. Lim, D. Y. Kang, M. Zimmermann, L. Zhang, J. Wang, *Angew. Chem., Int. Ed.* **2011**, *50*, 4161.
- [8] L. Baraban, D. Makarov, R. Streubel, I. Moench, D. Grimm, S. Sánchez, O. G. Schmidt, *ACS Nano* **2012**, *6*, 3383.
- [9] S. Campuzano, J. Orozco, D. Kagan, M. Guix, G. Gao, M. Sattayasamitsathit, J. C. Claussen, A. Merkoçi, J. Wang, *Nano Lett.* **2012**, *12*, 396.
- [10] L. Baraban, S. M. Harazim, S. Sánchez, O. G. Schmidt, *Angew. Chem., Int. Ed.* **2013**, *52*, 5552.
- [11] S. Sánchez, L. Soler, J. Katuri, *Angew. Chem., Int. Ed.* **2015**, *54*, 1414.
- [12] D. Pantarotto, W. R. Browne, B. L. Feringa, *Chem. Commun.* **2008**, *10*, 1533.
- [13] J. R. Howse, A. J. Ryan, R. A. L. Jones, R. Vafabakhsh, T. Gough, R. Golestanian, *Phys. Rev. Lett.* **2007**, *99*, 048102.
- [14] F. Kümmel, P. Shabestari, C. Lozano, G. Volpe, C. Bechinger, *Soft Matter* **2015**, *11*, 6187.
- [15] L. Baraban, R. Streubel, D. Makarov, L. Han, D. Karnaushenko, O. G. Schmidt, G. Cuniberti, *ACS Nano* **2013**, *7*, 1360.
- [16] J. Volpe, I. Buttinoni, D. Vogt, H.-J. Küppererand, C. Bechinger, *Soft Matter* **2011**, *7*, 8810.
- [17] H. H. Wensink, H. Loewen, *Phys. Rev. E* **2008**, *78*, 031409.
- [18] R. Golestanian, *Phys. Rev. Lett.* **2009**, *102*, 188305.
- [19] A. Solovev, W. Xi, D. Gracias, S. M. Harazim, C. Deneke, S. Sánchez, O. G. Schmidt, *ACS Nano* **2012**, *6*, 1751.
- [20] a) L. Baraban, D. Makarov, O. G. Schmidt, G. Cuniberti, P. Leiderer, A. Erbe, *Nanoscale* **2013**, *5*, 1332; b) I. S. M. Khalil, V. Magdanz, S. Sanchez, O. G. Schmidt, S. Misra, *Int. J. Adv. Rob. Syst.* **2015**, *12*, 2.
- [21] W. Gao, J. Wang, *ACS Nano* **2014**, *8*, 3170.
- [22] W. Gao, J. Wang, *Nanoscale* **2014**, *6*, 10486.
- [23] A. A. Solovev, Y. Mei, E. B. Urena, G. Huang, O. G. Schmidt, *Small* **2009**, *14*, 1688.
- [24] Y. Li, J. Wu, Y. Xie, H. Ju, *Chem. Commun.* **2015**, *51*, 6325.
- [25] V. Garcia Gradilla, J. Orozco, S. Sattayasamitsathit, F. Soto, F. Kuralay, A. Pourazary, A. Katzenberg, W. Gao, Y. Shen, J. Wang, *ACS Nano* **2013**, *7*, 9232.
- [26] A. Ghosh, P. Fischer, *Nano Lett.* **2009**, *9*, 2243.
- [27] W. Gao, D. Kagan, O. S. Pak, C. Clawson, S. Campuzano, E. Chuluun-Erdene, E. Shipton, E. E. Fullerton, L. Zhang, E. Lauga, J. Wang, *Small* **2012**, *8*, 460.
- [28] L. Baraban, M. Tasinkevych, M. N. Popescu, S. Sánchez, S. Dietrich, O. G. Schmidt, *Soft Matter* **2012**, *8*, 48.
- [29] A. Snezhko, I. S. Aranson, *Nat. Mater.* **2011**, *10*, 698.
- [30] P. K. Ghosh, V. R. Misko, F. Marchesoni, F. Nori, *Phys. Rev. Lett.* **2013**, *110*, 268301.
- [31] M. Medina-Sánchez, L. Schwarz, A. K. Meyer, F. Hebenstreit, O. G. Schmidt, *Nano Lett.* **2016**, *16*, 555.
- [32] S. Das, A. Garg, A. I. Campbell, J. Howse, A. Sen, D. Velegol, R. Golestanian, S. J. Ebbens, *Nat. Commun.* **2015**, *6*, 8999.
- [33] J. Simmchen, J. Katuri, W. E. Uspal, M. N. Popescu, M. Tasinkevych, S. Sánchez, *Nat. Commun.* **2016**, *7*, 10598.
- [34] A. Demortière, A. Snezhko, M. V. Sapozhnikov, N. Becker, T. Proslier, I. S. Aranson, *Nat. Commun.* **2014**, *5*, 3117.
- [35] M. N. Popescu, S. Dietrich, M. Tasinkevych, J. Ralston, *Eur. Phys. J. E* **2010**, *31*, 351.
- [36] M. Gai, J. Frueh, T. Si, N. Hu, G. B. Sukhorukov, Q. He, *Colloids Surf, A* **2016**, (accepted), doi: 10.1016/j.colsurfa.2016.04.042.
- [37] M. Gai, J. Frueh, N. Hu, T. Si, G. B. Sukhorukov, Q. He, *Phys. Chem. Chem. Phys.* **2016**, *18*, 3397.
- [38] C. Tscheik, I. E. Blasig, L. Winkler, *Tissue Barriers* **2013**, *1*, e24565.
- [39] A. Pathak, S. Kumar, *PNAS* **2012**, *109*, 10334.
- [40] J. Kreuter, *Colloidal Drug Delivery Systems*, CRC Press, New York **1994**.
- [41] D. J. Irvine, *Nat. Mater.* **2011**, *10*, 342.
- [42] R. Micheletto, H. Fukuda, M. A. Ohtsu, *Langmuir* **1995**, *11*, 3333.
- [43] L. Baraban, D. Makarov, M. Albrecht, N. Rivier, P. Leiderer, A. Erbe, *Phys. Rev. E* **2008**, *77*, 031407.
- [44] S. Ebbens, R. A. L. Jones, A. J. Ryan, R. Golestanian, J. R. Howse, *Phys. Rev. E* **2010**, *82*, 015304.
- [45] D. Takagi, A. B. Braunschweig, J. Zhang, M. J. Shelley, *Phys. Rev. Lett.* **2013**, *110*, 038301.
- [46] J. Burdick, R. Laocharoensuk, P. M. Wheat, J. D. Posner, J. Wang, *J. Am. Chem. Soc.* **2008**, *130*, 8164.
- [47] R. Greiner, M. Allerdissen, A. Voigt, A. Richter, *Lab Chip* **2012**, *12*, 5034.

Received: June 19, 2016

Revised: August 16, 2016

Published online: